Reactive power correction for an inductive power transfer system for EV application: Circuit and Control

S G Cimen, A. Popp, B Schmuelling

University of Wuppertal, Rainer-Gruenter-Str. 21, 42119 Wuppertal, Germany, cimen@uni-wuppertal.de

Keywords: Inductive power transfer, wireless EV charging, electromagnetic coupling, frequency control.

Abstract

A resonant circuit topology is generally applied in inductive power transfer (IPT) systems for electric vehicle battery charging to minimise the switching losses of IGBT. Various IPT systems under development ensure high-efficiency, if there is no misalignment. Each park process can cause high power losses due to a new resonance frequency, which occurs as a result of changing inductances, if the coils have misalignment. Power losses of IGBT soft switching can be reduced by tuning the operating frequency. Therefore, in this paper, a hardware for the frequency control of IPT system is developed, in which the hardware approximates operating frequency to the resonance frequency. In the software, the elimination of the bifurcation phenome is considered. An IPT system with a series-series compensated topology is used for laboratory setup.

1 Introduction

Wireless inductive power transfer (WIPT) is an established technology that uses high frequency electromagnetic field to transfer the electrical energy from a stationary electricity source to movable consumers over a large air gap. IPT has been successfully used for medical devices for the supply of sensor modules or for consumer electronics, such as mobile phones and electric tooth brushes [1-7].

Over the last few years, the application of the IPT technology as a charging method for the traction batteries of electric vehicles (EV) and hybrid electric vehicles (HEV) has seen an explosion in research and development in academic and industry sector [8-16]. This technique allows for a simple and reliable charging process. Increasing user-friendliness, comfort as well as associated automation of charging play an important role for the deployment of this technology. These systems provide an aesthetic way with more safety and more convenience compared to conductive power transfer systems. Furthermore, it is accessible to physically impaired users (barrier-free use) [17]. It is assumed that automatic inductive charging will improve the user acceptance of electric vehicles.

2 Proposed control strategy

Using a higher transmission frequency can increase the output power and the power efficiency of an inductive power transfer system, if the coils are on resonance. The power transmitted to the secondary side drops as either one of the coils is detuned from resonance [18,19]. Additionally, the utilisation of higher switching frequencies increases the transistor switching losses.

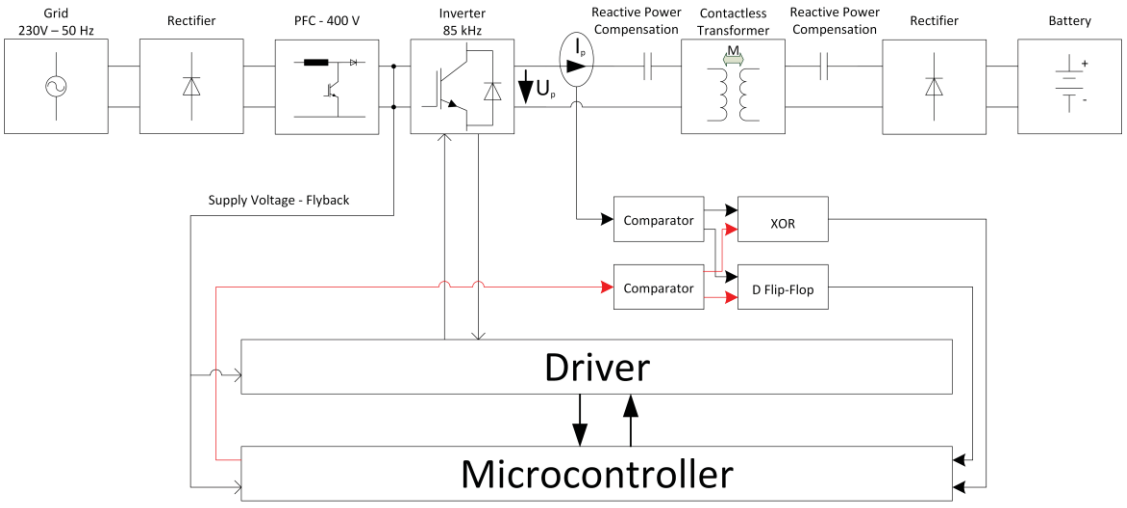

Fig. 1. Schematic of the proposed IPT System

In this work, a hardware for the frequency control of a 3kW IPT is investigated. A schematic of the required components is shown in Fig. 1. The IPT System is not investigated in detail in this paper. In these systems, the primary current shows a sinusoidal waveform and the primary voltage has a square waveform as forced by the switching procedure of the primary inverter. The phase angle between primary- voltage and current is nearly zero, if primary coil has exactly tuned with secondary coil and no misalignment exists. Due to horizontal and vertical misalignments and component tolerances caused by age, the transmission parameters can vary. This changing can be compensated by additional capacitance or by a newly adjusted operating frequency. For this adjustment the knowledge of phase angle between primary voltage and primary current is necessary [20].

The exclusive OR gate (XOR) produces a high-level signal during the displacement of the phase. The function of the transparent D Flip-Flop (DFF) is to determine whether it is inductive or capacitive. Depending on the signals produced by the XOR gate and the D-Flip-Flop, the controller updates the frequency. It generates the gate signal to drive the full-bridge configuration.

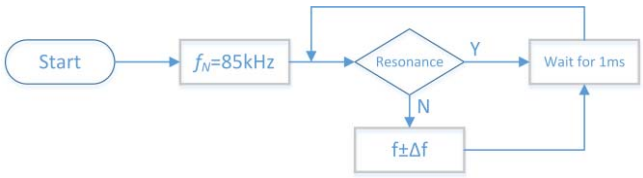

Fig. 2. Block diagram of the proposed circuit.

The zero crossing detection should be realised by a comparator circuit utilising high speed comparators before being sent to the microcontroller. The output signals of the comparator circuit can be filtered by Schmitt Triggers to avoid noise and to prevent uncontrolled switching.

The following logic makes a comparison. The output of the XOR-gate gives an insight into whether, there is a phase displacement or not. As aforementioned, the DFF gives information regarding the type of displacement (inductive or capacitive).

It is necessary to distinguish and to analyse the following cases:

- No phase shift
- Capacitive behaviour
- Inductive behaviour

3 Hardware

Fig. 2 illustrates the proposed system for the frequency control. The proposed circuit should carry out a comparative analysis of primary voltage and primary current, and it should be able to output phase shift, as well as sign (inductive, capacitive). Therefore, the circuit receives the voltage and

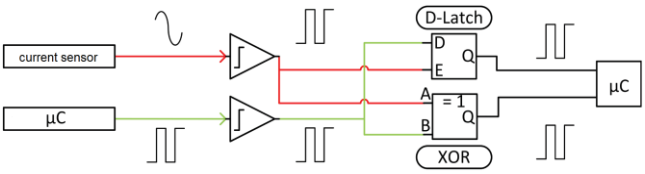

Fig. 3. Block diagram of the proposed circuit.

current curves as input. Due to the compensation of the coils that is switched resonant, the inductive transmission path behaves as an ohmic load, which causes a sinusoidal current to occur on the primary coil. The change in the voltage over time can be read by the microcontroller. Therefore, it can be captured directly by the microcontroller without galvanic connection to the high-voltage section. Due to the high switching frequencies at which the inverter operates, it is necessary to use a high speed comparator for the zero crossing stage. Following this, both output signals of the comparators are evaluated by the digital logic, switching states of which are listed in Table 1, whereby Q_0 indicates the state of the output one set-up time prior to the High-to-Low E transition. The phase shift is determined by XOR-gate. If both comparator signals are simultaneously high or low, this state is considered as resonant (no phase shift) according to Table 1 (a). At the same time, sign of the phase shift is determined by DFF. The corresponding signs are provided in the following function Table 1 (b).

A	*B*	*Q*
0	0	0
0	1	1
1	0	1
1	1	0

(a)

E	*D*	*Q*
0	0	Q_0
0	1	Q_0
1	0	0
1	1	1

(b)

Table 1: Function table for (a) the XOR-gate and (b) the DFF.

For the current measurement, a highly dynamic magneto resistive current sensor CMS3015 made by Sensitec is deployed. The gate signal for the IGBTs, which indicates the primary voltage, will be directly used for the phase angle analysis. The microcontroller is able to change the frequency in steps of 50 Hz and is programmed to adjust the initial operating frequency to 85 kHz.

4 Software

In this paper, an ARM Cortex F4, which is a high performance embedded processor with DSP instructions developed for digital controls, is used. The working frequency

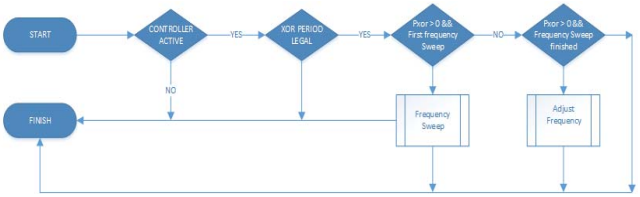

Fig. 4. Program sequence.

of the Controller is 168 MHz.

The nominal frequency (85 kHz) for the drivers of the IGBT full bridge configuration is produced through hardware PWM, which does not reduce the computation power of the Controller in a manner like a software PWM does.

Frequency and duty cycle of the XOR and DFF are calculated by a PWM Capture input Module of the microcontroller. This method is preferable to the acquisition of the PWM Signals by an analogue-digital-converter (ADC) because of the multiple cycles it takes to convert the input signal. Frequency and duty cycle of every detected signal are saved to compare, if there is any change in the last detected values. To gain further accuracy, the average over several acquisition cycles is taken as base for further calculations.

The controller initializes with a frequency of 85 kHz. Based on an internal timer of the ARM, the control sequence is carried out every one millisecond. The program sequence is depicted in Figure 3. To check for a legal signal, the frequency of the XOR is at the beginning of the control scheme evaluated. A legal period of the XOR is characterized by a doubled nominal frequency. If there is a legal signal and a variation of the phase (between the voltage and the current) that is indicated through the duty cycle of the XOR, the controller has to distinguish between two different cases.

In the first case, the controller sets the frequency to the lowest configured frequency (80 kHz). The frequency is now raised and the DFF is checked for a change of its sign. Based on the idea of bifurcation, there are only three zero crossings possible: at a lower point of resonance frequency, at an upper point of resonance frequency or even at the resonance frequency. Every detected zero crossing point is saved. When the controller reaches the highest set frequency on its sweep, the zero crossings recorded are checked. The most important point is, where the phase displacement from inductive to a capacitive phase displacement takes place. In the case of a bifurcation, it is a unique point. For more information about bifurcation, see [9, 10, 11, 21]. The active frequency is used as an operating frequency.

5 Results

In order to ensure that the results are correctly monitored and evaluated by the microcontroller, a PWM signal is generated with the frequency generator and it is monitored by an oscilloscope. During the measurement, the frequency of the frequency generator is changed gradually. The results measured by the oscilloscope deviate constant 2 Hz from the value of the frequency generator, which may occur because of parasitic noise of wires. Moreover, the measurements of the microcontroller vary up to 9 Hz, which corresponds to a relative deviation of up to 0.01%, as can be seen in Fig. 15.

Fig. 6 indicates the absolute deviations of the results related to different duty-cycles, whereby the frequency of the

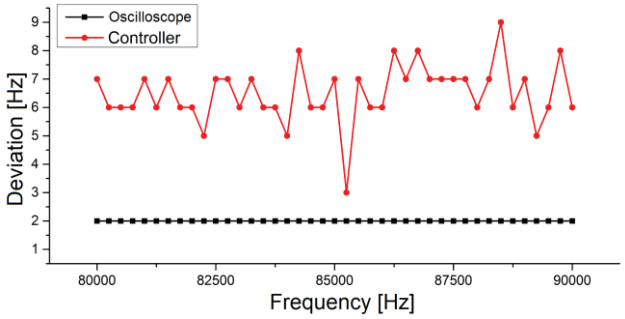

Fig. 5. Results of PWM signals measured by an oscilloscope and the microcontroller, when changing the frequency.

frequency generator is held constant at 85 kHz and only the duty-cycle is varied.

In a final step, the accuracy of the controller needs to be examined for the across the spectrum of the phase shift. For this, two PWM signals with the nominal frequency f_N are generated by the microcontroller. The signal which should present the current is gradually delayed, as a result of which the IPT system shows a capacitive behaviour. Here the output signals of XOR-gate and DFF are detected. The results are shown in Fig. 7 and Fig. 8. The horizontal axis shows the

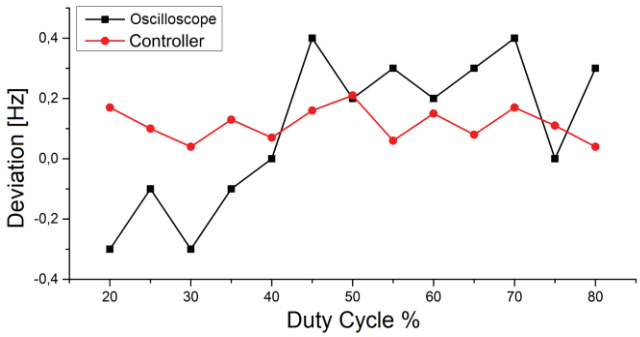

Fig. 6. Results of PWM signals measured by an oscilloscope and the microcontroller, when changing the duty-cycle at 85 kHz.

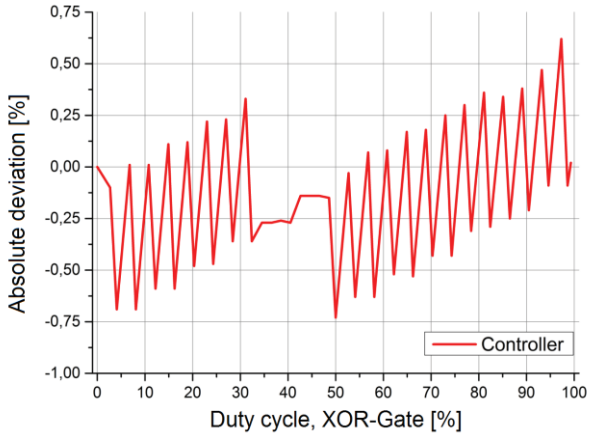

Fig. 7. Absolute deviation of the XOR-gate measurements of microcontroller from an oscilloscope.

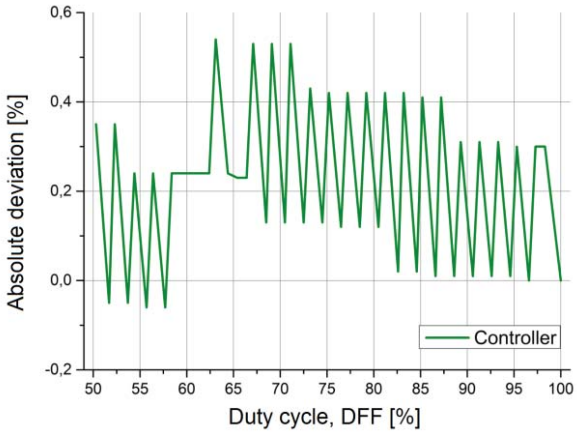

Fig. 8. Absolute deviation of the DFF measurements of microcontroller from an oscilloscope.

duty cycle of XOR-gate or DFF and the vertical axis indicates the absolute deviation of the measurements of the microcontroller from the measurements of the oscilloscope. Measured values of XOR-gate present on average a difference by ±0.3% and for the DFF a derogation by ±0.23%.

The final results of three cases that have been discussed in this paper are shown in Fig. 9, Fig. 10 and Fig 11. The experimental results are consistent with the expectations. It is conspicuous that the short impulses are to identify here for the case without phase shift, also resonant switch. However, these short impulses are not taken into account by microcontroller, then these do not represent a phase shift.

As shown in Fig. 10, the frequency of the signal produced by the XOR-gate is doubled. The phase shift between current and voltage can be seen by the yellow trace. The duty cycle shown by the green trace indicates an inductive behaviour.

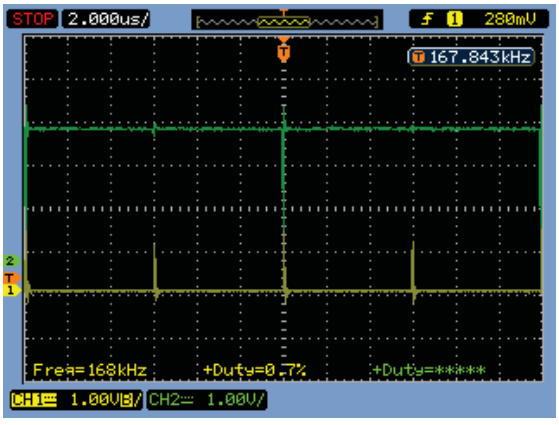

Fig. 9. Signal forms without phase shift, CH1 represents the output signal of XOR-gate and CH2 shows the output signal of DFF.

Fig. 11 shows waveforms indicating capacitive behaviour of the system. As previously mentioned, the XOR-gate shows the phase shift. It presents an expected signal due to its doubled frequency. Compared to the inductive behaviour, the duty cycle of the DFF is now greater than 50%.

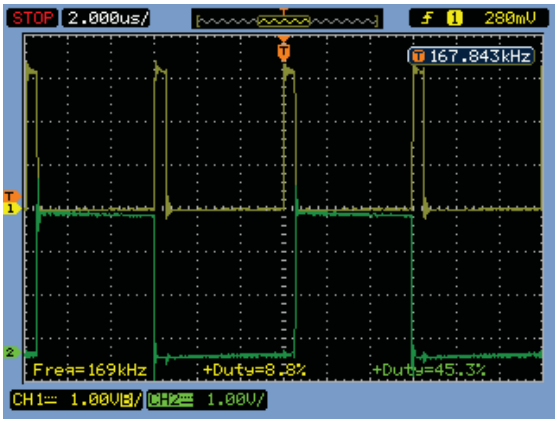

Fig. 10. Signal forms for the inductive behaviour, CH1 represents the output signal of XOR-gate and CH2 shows the output signal of DFF.

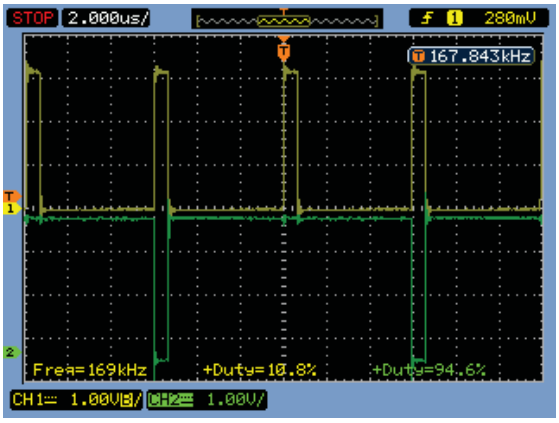

Fig. 11. Signal forms for the capacitive behaviour, CH1 represents the output signal of XOR-gate and CH2 shows the output signal of DFF.

6 Conclusion

This paper summarises the hardware and the software for the proposed frequency control of an IPT. Hardware and software, which were tested by use of laboratory setup, are shown and validated by experimental results.

The hardware and software presented here allow the controller to tune a detuned system, whether it has a capacitive or inductive displacement, back to resonance, so that the transmission parameters e.g. forced by misalignment of the coils can be adjusted.

In achieving more efficient for IPTs, the perception and acceptance of automatic noncontact-charging stations will rise and hence promote e-mobility.

References

[1] M. Ghovanloo, S. Atluri, "A wide-band power-efficient inductive wireless link for implantable microelectronic devices using multiple carriers," *IEEE Trans. on Circuits and Systems*, vol. 54, no. 10, pp. 2211-2221, 2007.

[2] C. M. Zierhofer, E. S. Hochmair, "Geometric approach for coupling enhancement of magnetically coupled coils," *IEEE Trans. on Biomedical Engineering*, vol. 43, no. 7, pp. 708-714, 1996.

[3] C. Reinhold, P. Scholz, W. John and U. Hilleringmann, "Efficient antenna design of inductive coupled RFID-systems with high power demand," *Journal of Communications*, vol. 2, no. 6, pp. 14-23, 2007.

[4] E. Waffenschmidt and T. Staring, "Limitation of inductive power transfer for consumer applications," *13th Eurpean Conference on Power Electronics and Applications (EPE)*, 2009.

[5] W. Kyung, P. H. Seok, C. Y. Hyun, and K. K. Ho, "Contactless Energy transmission system for linear servo motor," *IEEE Transactions on Magnetics,* vol. 41, no. 5, pp. 1596-1599, 2005.

[6] C.-H. Hu, C.-M. Chen, Y.-S. Shiao, T.-J. Chan, L.-R. Chen, "Development of a universal contactless charger for handheld devices," in *Proc. IEEE Ind. Electron. Conf. Expo., Int. Symp.,* pp. 99-104, 2008.

[7] C.-G. Kim, D.-H. Seo, J.-S. You, J.-H. Park, B.-H. Cho, "Design of a contactless battery charger for cellular phone," in *Proc. IEEE 15th Annu. Appl. Power Electron. Conf. Expo.,* vol. 2, pp. 769-773, 2000.

[8] B. Schmuelling, S. G. Cimen, T. Vosshagen, F. Turki, "Layout and operation of a non-contact charging system for electric vehicles," *Power Electronics and Motion Control Conference (EPE/PEMC),* pp. LS4d.4-1-LS4d.4-7, 2012.

[9] S. G. Cimen and B. Schmuelling, "A dynamic model of the bidirectional inductive power transfer system for electric vehicles," *16th Eurpean Conference on Power Electronics and Applications (EPE'14-ECCE)*, 2014.

[10] B. Schmuelling, S. G. Cimen, and J. Demtroeder, "Comparative Study of the Transmission Characteristic of Unequal Compensated Inductive Power Supply Systems for Electric Vehicles," *Przeglad Elektrotechniczny*, 91(3):1-4, ISSN: 0033-2097, 2015.

[11] S. G. Cimen, A. Pfannkuchen, B. Schmuelling, "Compensation Considerations for Bidirectional Inductive Charging Systems of Electric Vehicles with Coil Positioning Flexibility," *IEEE Trans. on Magnetics,* vol. 52(3): 1-4, 2016.

[12] M. Budhia, J. T. Boys, G. A. Covic, C.-Y. Huang, "Development of a Single-Sided Flux Magnetic Coupler for Electric Vehicle IPT Charging Systems," *IEEE Trans. on Ind. Electron.,* vol. 60, no. 1 pp. 318-328, 2013.

[13] G. Covic and J. Boys, "Modern trends in inductive power transfer for transportation applications," *IEEE J. Emerg. Sel. Topics Power Electron.,* vol. 1, no. 1, pp. 28-41, 2013.

[14] S. Lee, J. Huh, C. Park, N.-S. Choi, G.-H. Cho, C.-T. Rim, "On-line electric vehicle using inductive power transfer system," in *Proc. IEEE Energy Convers. Congr. Expo.,* pp. 1598-1601, 2010.

[15] J. Miller, O. Onar, C. White, S. Campbell, C. Coomer, L. Seiber, R. Sepe, A. Steyerl, "Demonstrating dynamic wireless charging of an electric vehicle: The benefit of electrochemical capacitor smoothing," *IEEE Power Electron. Mag,* vol 1, no. 1 pp. 12-24, 2014.

[16] F. Risch, S. Guenther, J. Franke, "Production concepts for inductive power transfer systems for electric vehicles," *2nd Electric Drives Production Conf. (EDPC),* pp. 1-7, 2012.

[17] S. G. Cimen, A. Popp, B. Schmuelling, "An inductive power transfer system for electric vehicles with a safe and modular primary side inverter," *8th IET International Conf. on Power Electronics, Machines and Drives (PEMD),* 2016.

[18] A. Kurs, A. Karalis, R. Moffatt, J.D. Joannopoulos, P. Fisher, M. Soljacic, "Wireless power transfer via strongly coupled magnetic resonances," *Science Mag.,* vol. 317, no. 5834, pp. 83-86, 2007.

[19] D. A. G. Pedder, A. D. Brown, J. A. Skinner, "A contactless electrical energy transmission system," *IEEE Trans. On Industrial Electronics,* vol. 46, no. 1, pp. 23-30, 1999.

[20] R. Czainski, " Robuste Strom-Phasenwinkelmessung für CPS-Frequenzumrichter mit optimiertem Ausgangs-leistungsfaktor", [Online], URL: https://www.tu-braunschweig.de/Medien-DB/imab/09-Jahresberichte/2009/05_Czainski_2009.pdf.

[21] S. G. Cimen and B. Schmuelling, "Frequency Bifurcation Study of an Inductive Power Transmission System," *4th International Conference on Power Engineering, Energy and Electrical Drives, (POWERENG),* 2013.